JACS
JOURNAL OF THE AMERICAN CHEMICAL SOCIETY
Article
pubs.acs.org/JACS

Conjugated Covalent Organic Frameworks via Michael Addition−Elimination

M. Rajeswara Rao,[†] Yuan Fang,[†,‡] Steven De Feyter,[‡] and Dmitrii F. Perepichka*[,†]

[†]Department of Chemistry, McGill University, 801 Sherbrooke Street West, Montreal, Quebec H3A 0B8, Canada
[‡]Division of Molecular Imaging and Photonics, Department of Chemistry, KU Leuven − University of Leuven, Celestijnenlaan 200 F, B-3001 Leuven, Belgium

Supporting Information

ABSTRACT: Dynamic covalent chemistry enables self-assembly of reactive building blocks into structurally complex yet robust materials, such as covalent organic frameworks (COFs). However, the synthetic toolbox used to prepare such materials, and thus the spectrum of attainable properties, is very limited. For π-conjugated COFs, the Schiff base condensation of aldehydes and amines is the only general dynamic reaction, but the resulting imine-linked COFs display only a moderate electron delocalization and are susceptible to hydrolysis, particularly in acidic conditions. Here we report a new dynamic polymerization based on Michael addition−elimination reaction of structurally diverse β-ketoenols with amines, and use it to prepare novel two-dimensional (2D) π-conjugated COFs, as crystalline powders and exfoliated micron-size sheets. π-Conjugation is manifested in these COFs in significantly reduced band gap (1.8−2.2 eV), solid state luminescence and reversible electrochemical doping creating midgap (NIR absorbing) polaronic states. The β-ketoenamine moiety enables protonation control of electron delocalization through the 2D COF sheets. It also gives rise to direct sensing of triacetone triperoxide (TATP) explosive through fluorescence quenching.

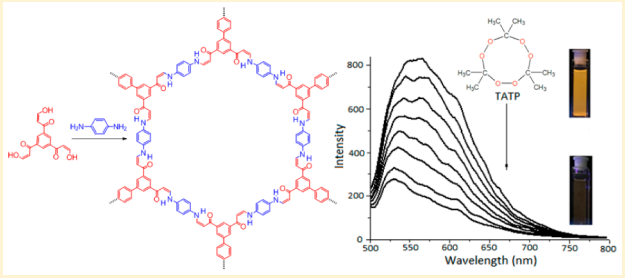

INTRODUCTION

Covalent organic frameworks (COFs) are porous crystalline solids obtained by 2D or 3D polymerization of organic building blocks.[1] They emerge as new promising materials for gas[2] and energy storage,[3] catalysis,[4] and semiconducting device applications.[5] Achieving crystalline order in COFs relies on the reversibility of the used chemical reaction; carrying out the polymerization under dynamic equilibrium conditions allows the system to self-assemble toward thermodynamic minimum, via error-correction mechanism (i.e., unlinking and relinking improperly connected building blocks).[1] However, only a handful of reactions[1e] are sufficiently dynamic to enable such mechanism: boronic acid self-condensation and polycondensation with aromatic diols,[1,6] aldehyde/amine condensation (Schiff base reaction),[7] nitroso dimerization[8] and imidation[9] reactions. Among these, Schiff base reaction forming imine bonds is currently the only dynamic covalent chemistry suitable for making π-conjugated COFs.[10]

Electron delocalization in conventional, 1D π-conjugated polymers gives rise to their special optoelectronic properties, that are employed in organic light-emitting diodes, photovoltaics, photodetectors, field-effect transistors, sensors, etc.[11] Even more intriguing opportunities could be created if equally efficient electron delocalization in π-functional materials is extended in the second dimension.[12] These opportunities, however, are barely explored in COFs, although a significant progress has been made in 2D conjugated networks synthesized via surface-catalyzed polymerization and other nonequilibrium reactions.[13] Indeed, due to its high polarization, the imine linkage of Schiff base COFs is not very efficient in supporting π-delocalization between the connected units, and most COFs prepared via the dynamic covalent chemistry approach display a modest (0.2−0.3 eV) reduction in the bandgap in comparison to molecular reference compounds (Table S1).

Herein, we present a novel and general synthetic approach toward crystalline COFs with improved π-delocalization, using Michael addition−elimination reaction of β-ketoenols and aromatic amines (Scheme 1). The resulting β-ketoenamine linked COFs display an enhanced hydrolytic stability endowed by the intramolecular C═O···HN hydrogen bonding, and can be prepared from a broad variety of electrophilic and nucleophilic building blocks. The electron delocalization in these COFs leads to a pronounced band gap reduction (0.3−0.6 eV), reversible electrochemical doping, and light-emitting properties. The combination of the π-conjugation with specific host−guest interactions within the pores of the COF, gives rise to a remarkable sensing behavior. The fluorescence of **3BD** and **3′PD** is effectively quenched by the *direct* interaction with triacetone triperoxide (TATP). This is a notoriously dangerous explosive, but its detection is more challenging than that of common nitro explosives due to its relative chemical inertness

Received: November 28, 2016
Published: January 14, 2017

DOI: 10.1021/jacs.6b12005
J. Am. Chem. Soc. 2017, 139, 2421−2427

Scheme 1. Michael Addition−Elimination Reaction[a]

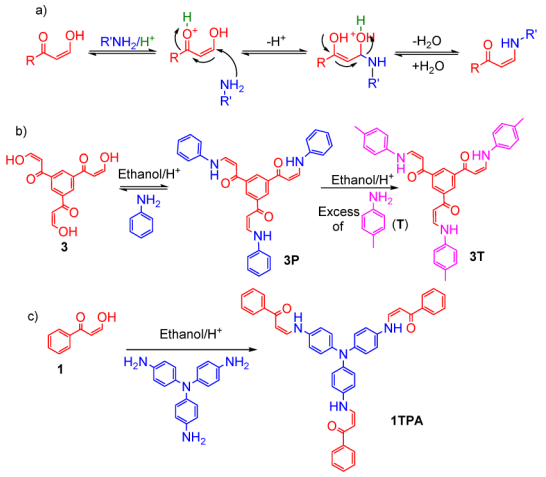

[a]Mechanistic pathway (a); synthesis and metathesis of enamines **3P** (b) and 1TPA (c).

(although a fluorescent detector for both, Fido Paxpoint, has already been commercialized by ICx Technologies[14]). We also note that the β-ketoenamine linker resembles that reported by Banerjee and co-workers[15] for a COF obtained via tautomerisation of β-hydroxyimine (prepared by Schiff base condensation). This transformation relied on the instability of 1,3,5-trihydroxysubstituted benzene ring and is thus limited to one particular building block (trihydroxytrimesic aldehyde). In contrast, our approach has a broad scope of electrophilic substrates, and we demonstrate its feasibility with four readily available β-ketoenol precursors.

RESULTS AND DISCUSSION

To demonstrate the diversity of our approach, we have synthesized four β-ketoenol-functionalized building blocks **1**−**3** and **3′** (Schemes 1, 2) in a one-step reaction of corresponding acetophenone precursors with ethyl formate (yield = 74−82%, SI). To verify the chemical selectivity and dynamic nature of the proposed Michael addition−elimination polymerization, we have studied an exchange reaction of the reference compound **3P** with toluidine (**T**). In situ NMR monitoring of a mixture of **3P** and **T** reveals a significant exchange over a course of few hours at room temperature in $CDCl_3$ (Figure S1). Furthermore, heating **3P** with an excess of **T** (80 °C, ethanol/catalytic amount of acid) leads to quantitative formation of **3T** (Figures 1, S2). These experiments show that the reaction is highly reversible, and potentially suitable for formation of COFs.

The COFs were synthesized by reacting di- and tritopic β-ketoenols (**2**, **3**, **3′**) with aromatic amines (**PD, BD, TPA**) at 130 °C in the presence of aqueous acetic acid (Scheme 2). The resulting orange (**3BD**, **3′PD**) to deep-red (**3PD** and **2TPA**)

Scheme 2. Synthesis of COFs via Michael Addition−Elimination under Solvothermal Conditions[a]

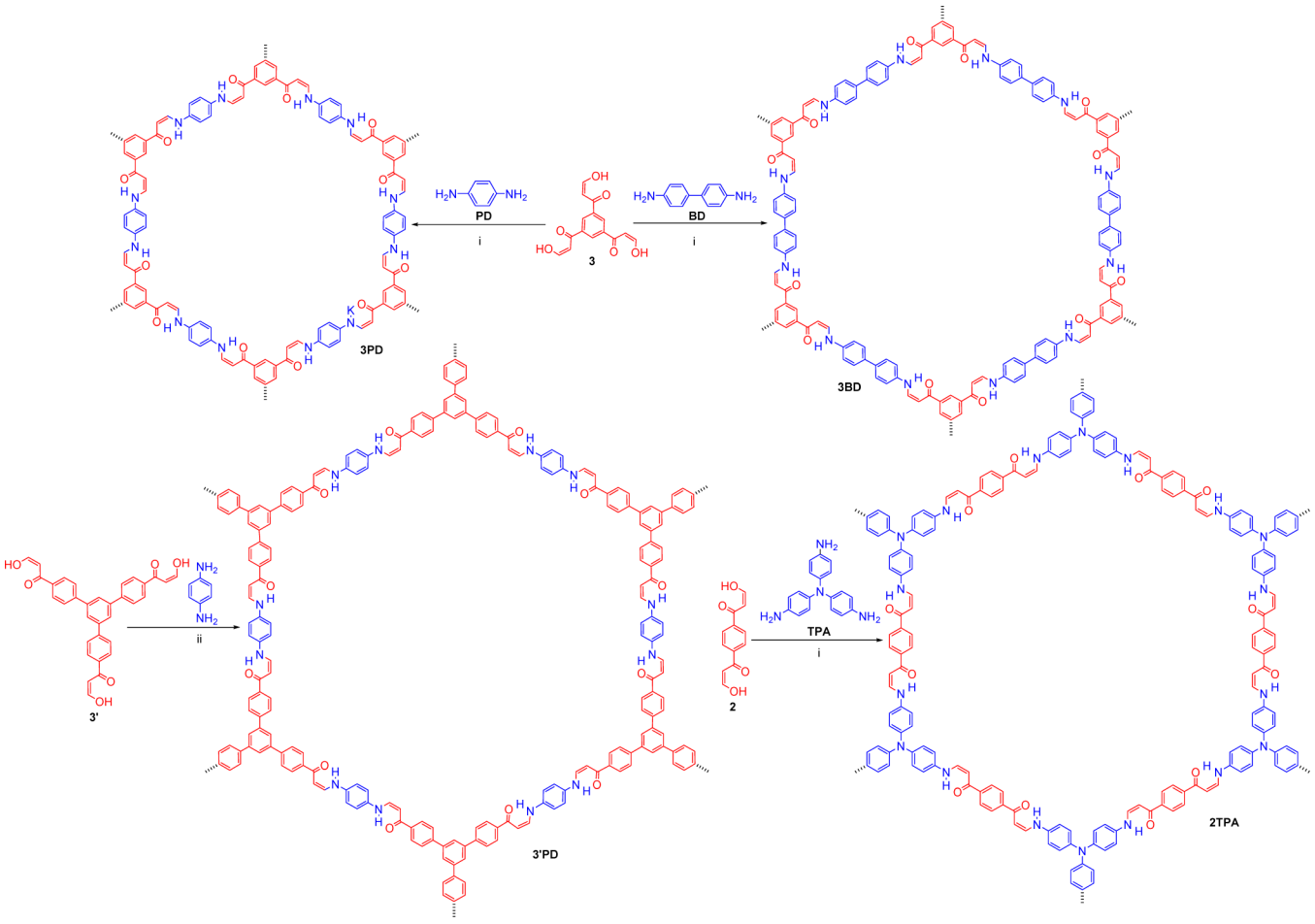

[a](i) 5/5/1 dioxane:mesitylene:6 M acetic acid; 130 °C/3 days; (ii) 5/100/1 dioxane:mesitylene:6 M aq. acetic acid; 130 °C/3 days.

DOI: 10.1021/jacs.6b12005
J. Am. Chem. Soc. 2017, 139, 2421−2427

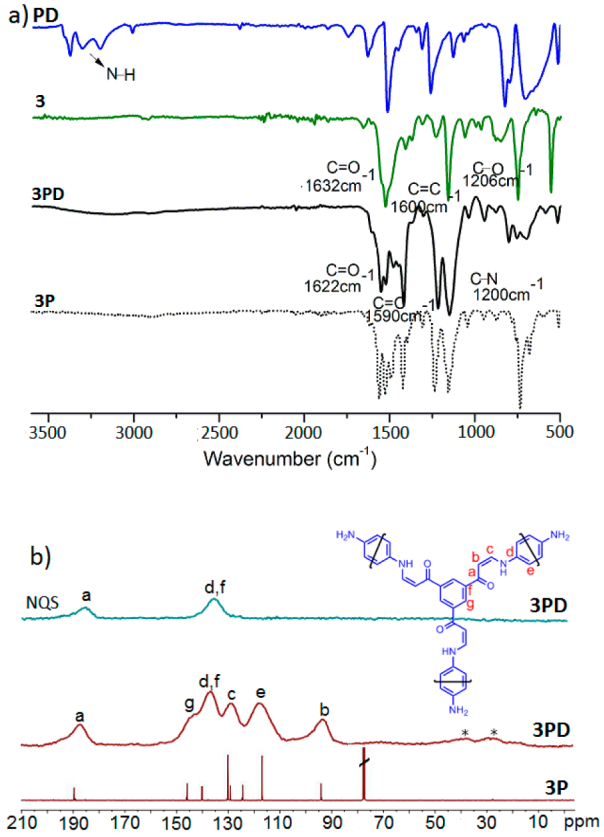

Figure 1. IR and NMR characterization of the COFs. (a) Comparison of the IR spectra of COF **3PD**, reference compound (**3P**) and building blocks (**3** and **PD**); (b) comparison of solid state ^{13}C cross-polarization magic angle spinning (CP-MAS) and NQS NMR spectra of **3PD** COF and solution ^{13}C NMR spectrum of **3P** reference. Asterisks indicate spinning side bands.

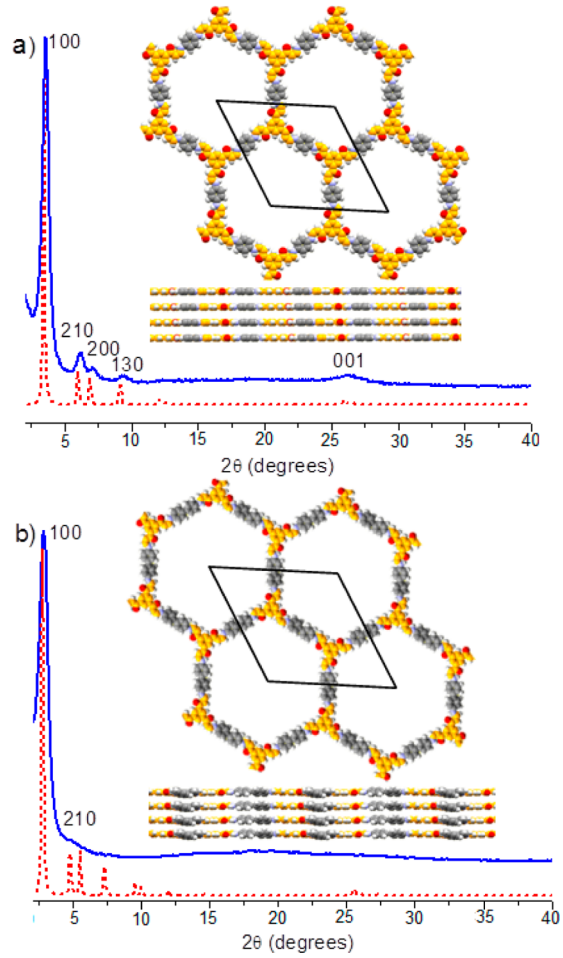

Figure 2. PXRD patterns and simulated crystal structures of COFs. Experimental PXRD of as-synthesized (solid lines) and simulated (broken lines) XRD pattern using the eclipsed AA stacking of **3PD** (a) and **3BD** (b). Inset shows the top and side views of the COFs structures. The simulated 2D unit cell parameters are $a = b = 29.7$ Å, $c = 3.4$ Å for **3PD**; $a = b = 37.4$ Å, $c = 3.4$ Å for **3BD**.

powders were filtered, purified by Soxhlet extraction (THF over 24 h) and dried under vacuum at 120 °C.

The infrared (IR) spectra of all synthesized COFs showed a complete disappearance of characteristic N−H stretching of the primary amines (3470 and 3420 cm^{-1}); the C−O stretching at ~1206 cm^{-1} is replaced by a new band at 1200 cm^{-1} attributed to the formed C−N bond (Figure 1a and Figures S3−S5). The overall IR spectra of the COFs closely resemble that of molecular reference compounds (**3P**, see Figure 3a; **2P** and **3′P**, Figure S3−S5). The chemical structures of the COFs were further confirmed by ^{13}C solid state NMR spectroscopy, and the signals were identified with the help of the ^{13}C nonquaternary suppression (NQS) measurements (Figures 1b and S6, S7). All COFs showed a characteristic signal at ~190 ppm, corresponding to the α,β-unsaturated carbonyl (C═O) carbon. The α-carbon signal (b) of ketoenamine in the COFs is shifted upfield to 93 ppm in comparison to ketoenol **3** (99 ppm), in line with the C−N linkage. All the signals are fully consistent with those of reference compounds (**3P**, Figure 1b; **3′P** and **2P**, SI).

Powder X-ray diffraction (PXRD) of the prepared COFs (Figure 2 and Figures S8−S11) reveals strong peaks at 2θ = 3.52° (24.5 Å), 2.90° (30.8 Å) and 2.29° (38.6 Å) for **3PD**, **3BD** and **3′PD**, respectively.[16] These correspond to (100) reflections defined by the periodicity of the covalent network. The broad peak at $2\theta \sim 26°$ for **3PD** corresponds to the (001) reflection, indicating an interlayer distance of ~3.4 Å. Higher order reflection peaks were also observed for **3PD** (Figure 2a) but not the other COFs, suggesting partial loss of crystallinity with increasing length of the linkers. The Scherrer analysis of (100) peak width for **3PD** suggests an average crystalline coherence length on the order of 10−15 nm. Density functional theory (DFT) calculations of 2D polymers[12b] corresponding to individual COF sheets were carried out under periodic boundary conditions (PBC), using the B3LYP functional. 3D models of COFs were built from the corresponding DFT-optimized 2D polymer sheets, assuming 3.4 Å van der Waals spacing between the covalent sheets, and using various stacking shifts. The simulated PXRD patterns of the resulting model in an eclipsed orientation (AA stacking with a small stacking shift, see SI) matched well the experimental data (Figure 2). In contrast, staggered (AB) orientations show significant deviations from the observed PXRD patterns (Figures S8−S11).

The permanent porosities were determined by Brunauer−Emmett−Teller (BET) method using N_2 adsorption at 77k, for supercritical CO_2 activated[17] COF samples. All COFs displayed reversible type−I isotherms with a very small hysteresis (Figures S12, S13). The smallest unit cell COF **3PD** revealed BET surface area of 505 m^2/g and pores volume of 0.36 cm^3 g^{-1} which is comparable to imine-linked COFs with similar unit

DOI: 10.1021/jacs.6b12005
J. Am. Chem. Soc. 2017, 139, 2421−2427

cell.[4a,15a] However, enlarging the unit cell by 0.75 nm in **3BD** unexpectedly led to a slightly lower BET surface area of 478 m^2/g, and even much lower porosity was revealed by the COFs **3′PD** and **2TPA** (Table S2). We also note that when the activation was carried out by simple vacuum drying (120 °C), ca. twice lower surface areas were measured for all COFs.

This strongly suggests that partial collapse of the framework takes place during the activation, and further optimization of the activation procedure might lead to higher open porosity.

Scanning electron microscopy (SEM) of as-prepared COF powders showed several hundred nm size globular particles with no clear signs of crystallinity (Figures 3a and S14–S17). A very different picture, however, emerges from the microscopy of exfoliated samples. Both transmission electron microscopy (TEM) and atomic force microscopy (AFM) measurement on exfoliated **3PD** samples prepared by sonication of ground COF powders in toluene reveals ∼half-micron large sheets with a uniform height in the range of 0.7–4.5 nm (Figures 3b–d and S18). This corresponds to a stack of ∼2–15 COF sheets. The apparent structural integrity of the covalent sheets on the order of hundreds of nm is not revealed in the SEM images, possibly due to their crumpling in the as-prepared COF powders. We note that single layers of 2D conjugated polymers are of interest for the potential graphene-like electron confinement effects and expected efficient charge transport properties.[12a] On-surface growth of such materials is an explosively growing research field,[13a–d] but is presently limited to metallic surfaces, which hampers their applications. In this respect, exfoliation of COFs[18,15b] provides an alternative approach to access such materials.

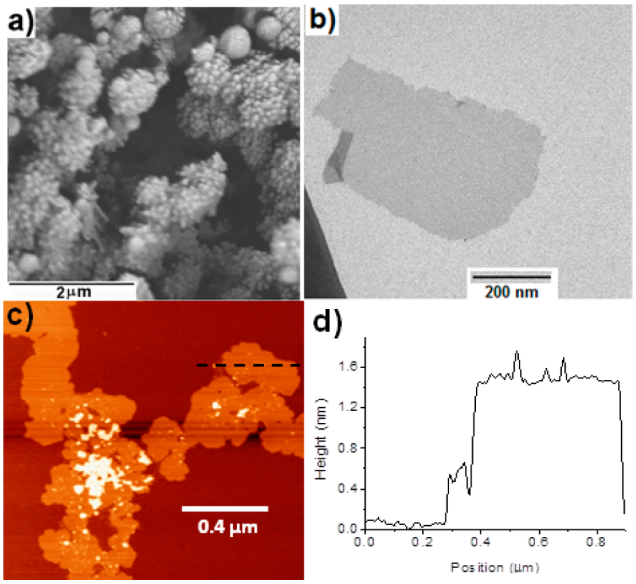

Figure 3. Morphology of 3PD. (a) SEM image of COF powder. (b) TEM image of a COF nanosheet exfoliated by sonication in toluene (c) AFM image of COF nanosheets on mica in water. (d) Cross-section analysis of (c).

Thermal gravimetric analysis (TGA) of the activated COFs showed an onset of thermal decomposition temperatures at ca. 300 °C (Figure S19). As earlier demonstrated for other COFs, intramolecular H-bonding can dramatically suppress hydrolysis of these materials.[10f,15a] Likewise, our COFs showed a remarkable hydrolytic stability in a strong acid (9 M HCl) as well as in hot water (50 °C) displaying no signs of decomposition in IR and PXRD analysis after over 1 week exposure. A partial loss in the PXRD signal intensity was noticed upon exposure of **3PD** to 9 M NaOH (but no discernible change in IR spectrum) which could be attributed to structural rearrangement induced by partial hydrolysis. A control experiment with Schiff base COF lacking H-bonding stabilization (**TFBPD**,[4a] prepared by condensation of 1,3,5-triformylbenzene and **PD**, see SI) hydrolyzes with complete dissolution in 9 M HCl within hours (Figures S20–S22).

Diffuse reflectance spectra of the synthesized COFs revealed a red absorption edge at ∼565–685 nm, corresponding to the optical band gap E_g of ∼2.2–1.8 eV (Figure 4a). **3PD** COF with the smallest unit cell has E_g = 2.03 eV; this is increased to E_g = 2.19 eV (**3BD**) and 2.17 eV (**3′PD**) upon introduction of additional phenylene links in the unit cell. Deplanarization of the polymer network due to Ph···Ph twist might be partially responsible for the increased band gap, although diminished conjugation is also theoretically predicted[12b] for fully planar 2D polymers networks upon extending the links between the nodes. On the other hand, introducing an electron-rich (triphenyl amine) unit in the covalent network of **2TPA** gives rise to contraction of E_g (1.79 eV), which is commonly observed in linear (1D) conjugated polymers with alternating D–A structure.[11]

Relative to molecular reference compounds **1TPA, 3P, 3′P** (representing 2D unit cells of these COFs), the band gap of COFs is contracted by 0.34–0.62 eV (Figure 4a, Table S2) due to π-delocalization through the polymer sheet. However, this is limited by cross-conjugation through the *meta*-connected benzene core of **3** and **3′** or through nitrogen lone pair of **TPA**. Nevertheless, the β-ketoenamine-based COFs show a lower band gap vs imine-based COFs, as revealed by comparing **3PD** (E_g = 2.03 eV) to corresponding imine linked **TFBPD** (E_g = 2.45 eV) (Figure S24).[4a] This could be attributed to the D–A interactions (carbonyl-amine) in the former.

The DFT calculations for individual 2D polymer sheets predict the same trend of band gap evolution: 3.16 eV for **3PD**; 3.27 eV for **3BD** and 3.18 eV for **3′PD**; and 2.67 eV for **2TPA**. In all four COFs, the HOMO is mostly centered over the arylamine moieties and appears increasingly localized with enlarging the unit cell of the COF (Figure S25–S28). However, the LUMO is delocalized through the entire network, with exception for **2TPA** where the electron-rich TPA units reveal very small LUMO density. This is not favorable for in-plane conductivity, a common problem for all reported COFs.

COFs **3BD** and **3′PD** exhibit orange luminescence in the solid state with a broad band at λ_{max} 547 and 560 nm (λ_{ex} 450 nm), respectively. These are bathochromically shifted vs reference compounds **3P** (λ_{max} 510 nm) and **3′P** (λ_{max} 480 nm) (Figure S29). The lifetime of the emission is very short (<0.5 ns) pointing to fluorescent nature of the process. Interestingly, the luminescence of dried COFs is visibly lower than that of dispersions in solvents (CH_2Cl_2, THF, diethyl ether, toluene etc.).

Fluorescence quenching of linear (1D) conjugated polymers in the presence of strong electron acceptors is one of the most attractive methods for detection of nitro-based explosives.[19] Charge-transfer interactions between a nitro acceptor and electron rich polymer, and efficient exciton diffusion through the polymer chain, lead to very high selectivity and sensitivity of this simple detection method. On the other hand, conventional conjugated polymers have no specific interactions with triacetone triperoxide (TATP), an extremely dangerous and

DOI: 10.1021/jacs.6b12005
J. Am. Chem. Soc. 2017, 139, 2421–2427

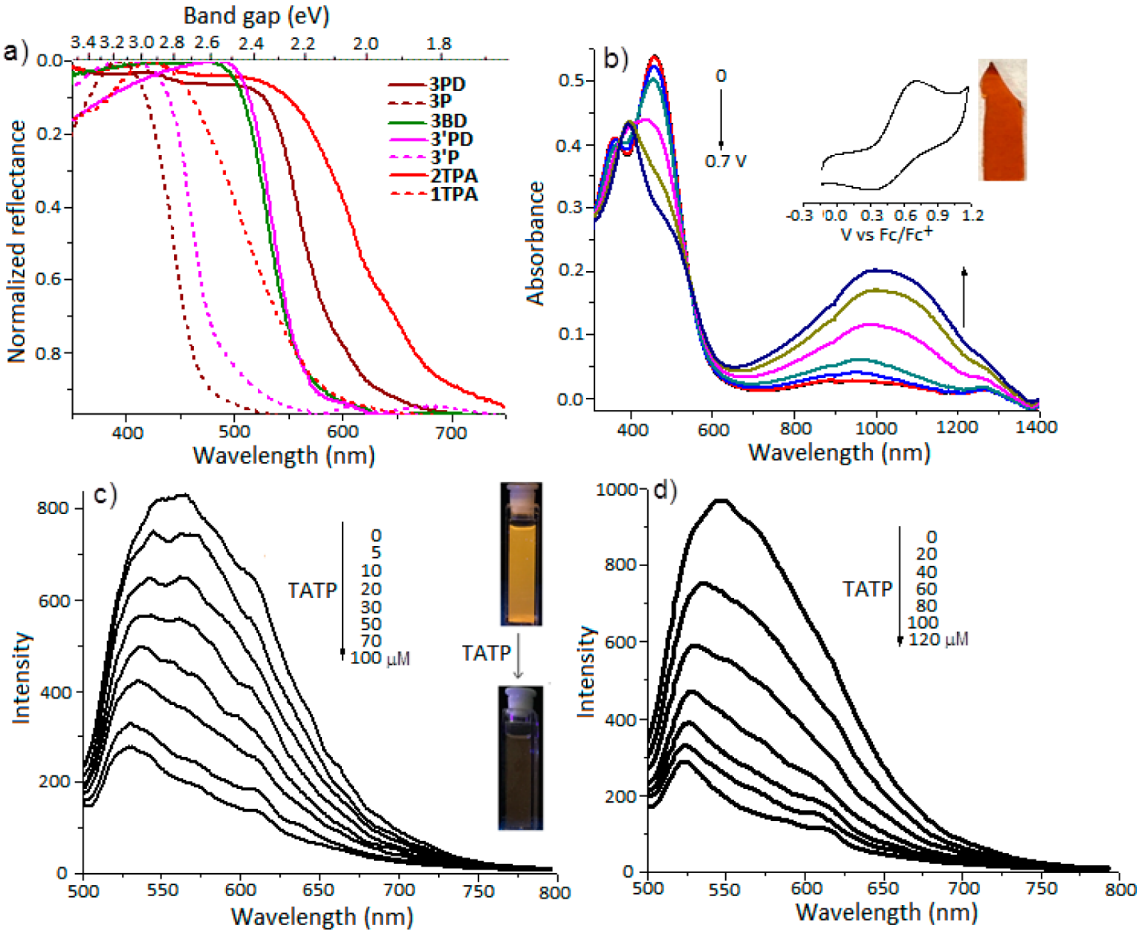

Figure 4. (a) Diffuse reflectance spectra of all COFs and their corresponding reference compounds. (b) Spectroelectrochemical measurements of **2TPA** (insets show the cyclic voltammogram and the photograph of COF-covered ITO electrode). Photoluminescence spectra of **3′PD** (c) and **3BD** (d) (λ_{ex} = 450 nm) dispersions in CH_2Cl_2 and fluorescence quenching in the presence of TATP (inset shows the photograph of **3′PD** dispersion, before and after adding TATP).

readily accessible explosive, implicated in many terrorist attacks. While a number of TATP detection methods have been reported and an already commercialized Fido Paxpoint is capable of detecting many explosives including TATP, most of these are based on detection of hydroperoxides, either present as impurities or generated in situ through chemical or photochemical treatment of TATP.[14,20]

Our COFs **3BD** and **3′PD** exhibit fluorescence quenching in the presence of both nitro- (picric acids, Figure S30) and peroxide-based (TATP) explosives. Titration of CH_2Cl_2 solution of TATP into suspension of **3BD** or **3′PD** (ca. 0.02 mg/mL) leads to a gradual decrease of the emission signal with a concomitant blue shift, and with detection on-set of ∼1 μM of TATP (Figures 4c,d and S31−S33). We note that while sensing of picric acid and other nitroaromatics by fluorescent COFs was reported,[21] TATP detection by COFs or other π-conjugated polymers is unprecedented. No acid treatment or photolysis, used to generate H_2O_2 in other sensing systems,[20] was applied. Furthermore, in these conditions (up to 1 mM concentration), neither H_2O_2 itself nor *t*-BuOOH quench the fluorescence of our COFs (Figures S35, S36). The direct energy or electron transfer from excited COFs to TATP is unlikely due to large optical gap (>3 eV) and very high LUMO of the latter. The observed fluorescence quenching can most probably be attributed to an oxidation of the enamine moiety by TATP, which is supported by the change of the color in these COFs (red-shift) in TATP solution (Figures S31, S32). Nevertheless, the environment of the COF pores controlling the interaction with TATP, while not yet fully understood, appears critically important. Indeed, control experiments with the oligomeric enamines **3P** and **3′P** showed no response to TATP (tested up to 1 mM).

Doping of conjugated polymers[22] is required to create free charge carriers and is an essential part in most of their device applications. However, the possibility of *reversible* doping in conjugated COFs is not yet well established. The only pertinent work we know of describes chemical *p*-doping of tetrathiafulvalene-containing COF using iodine.[23] Here, we present the first case of electrochemical doping of the **2TPA** COF. Films of **2TPA** were solvothermally grown on conductive ITO glass (Figure 4b, inset). Cyclic voltammetry of this sample reveals a quasi-reversible oxidation wave at E_{pa} ∼ 0.7 V that can be associated with electron loss from the **TPA** unit. Recording Vis-NIR absorption of this film upon progressive stepwise increase of the oxidation potential leads to attenuation of the 460 nm band corresponding to the neutral COF and the appearance of two new bands at λ_{max} 395 and 1020 nm (Figure 4b). On the basis of the topology of the HOMO (Figure S28), it is expected that the formed radical cations are primarily located on the TPA moieties, although the red shift of absorption of **2TPA**$^{\cdot+}$ (0.85 eV) relative to the reference compound **1TPA**$^{\cdot+}$ (1.03 eV Figure S38) suggests their appreciable interaction/delocaliza-

DOI: 10.1021/jacs.6b12005
J. Am. Chem. Soc. 2017, 139, 2421−2427

tion through the COF. The doping is completely reversible as evident by restoration of the original spectrum of the neutral COF upon applying a reductive potential (−0.5 V, Figure S39). **2TPA** can also be doped chemically (I_2 vapor), producing a very similar NIR absorption to the electrochemically doped films (Figure S40).

The ketoenamine moiety also allows to tune the π-conjugation via protonation (acid doping). Exposing COFs **3PD**, **3BD**, **3′PD** and **2TPA** to trifluoroacetic acid (TFA) leads to a red shift of their absorption bands by 150−200 nm (E_g = 1.45−1.81 eV, Figures S41, S42). This is attributed to enhanced electronic delocalization through the protonated ketoenamine bridge. Indeed, the efficient electron delocalization through the formally cross-conjugated β-ketoenamine moiety could be explained by the resonance contribution of the β-iminomethylene-enol tautomer that leads to partial bond length equalization across the link (Scheme 3).

Scheme 3. Tautomerism and Resonance Electron Delocalization in β-Ketoenamine Links[a]

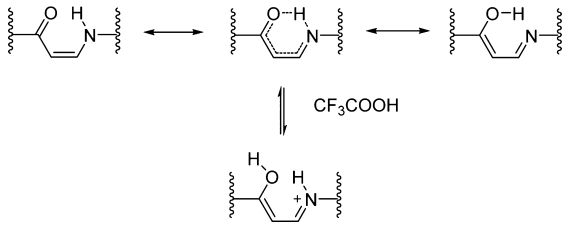

[a]Intramolecular proton transfer converts cross-conjugation of β-ketoenamine (left) into direct conjugation of β-iminomethylene-enol (right). The latter resonance form is enforced by protonation (bottom).

Protonation of this link increases the contribution of the latter resonance form, enabling direct π-conjugation. In comparison, molecular references **2P**, **3P** and **3′P** show no noticeable color change and only a minor red shift of absorption upon exposure to TFA (by 15−20 nm, Figure S43), once again highlighting the optoelectronic effect of π-conjugation in our COFs.[24]

CONCLUSIONS

In summary, we have developed a new dynamic covalent polymerization based on Michael addition−elimination reaction of a series of aromatic β-ketoenols with arylamines. Applicable to a variety of easily accessible monomers, this reaction constitutes the third *general* methodology for preparation of crystalline porous covalent organic frameworks. Comparing to the other two reported families of COF (prepared by boronic acid and Schiff base condensation), the β-ketoenamine COFs exhibit much higher hydrolytic stability and provide a more efficient π-electron delocalization. The latter property is manifested in significant band gap reduction and reversible electrochemical doping creating NIR-absorbing midgap states. **3BD** and **3′PD** COFs are fluorescent and their emission is efficiently quenched in the presence of both nitroaromatic (picric acid) and peroxide (TATP) explosives. This fluorescent detection of TATP is direct (that is not mediated by hydroperoxides), although its precise mechanism is yet to be elucidated. Our synthetic strategy opens new opportunities to develop electronically functional COFs, and could enable new applications in semiconducting and sensing devices.

METHODS

3PD and **3BD**. Triketoenol **3** (35.0 mg, 0.121 mmol) and diamine **PD** (19.7 mg, 0.182 mmol) or **BD** (33.4 mg, 0.181 mmol) were suspended in a degassed mixture of 1,4-dioxane (3 mL), mesitylene (3 mL) and 6 M aq. acetic acid (0.5 mL) in a 12 mL high pressure glass vessel. The mixture was degassed for 10 min and tube was sealed and heated to 130 °C for 3 days. The precipitate was filtered and washed with 1,4-dioxane, water and acetone (10 mL each) and subjected to Soxhlet extraction with THF for 24 h to remove the trapped guest molecules. The powder was dried at 120 °C under vacuum overnight to yield **3PD** (35 mg, 83%) and **3BD** (40 mg, 78%) as red and orange solids, respectively.

2TPA was prepared using the above synthetic protocol, from diketoenol **2** (22.5 mg, 0.103 mmol) and triamine **TPA** (19.9 mg, 0.068 mmol). The COF was isolated as a red powder (27 mg, 84%).

3′PD was prepared using the above synthetic protocol except the solvent combination was changed to 1,4-dioxane (0.3 mL), mesitylene (5.7 mL) and 6 M acetic acid (0.5 mL), from triketoenol (**3′**) (30.0 mg, 0.058 mmol) and diamine **PD** (9.4 mg, 0.086 mmol). The COF was isolated as an orange powder (27 mg, 80%).

TATP and Picric Acid Sensing. Stock solutions (10 mM) of recrystallized TATP and commercial grade (Sigma-Aldrich) picric acid were prepared in dichloromethane. A homogeneous dispersion of **3BD** or **3′PD** (0.02 mg/mL) in dichloromethane was made by sonication (10 min). The fluorescence titrations were carried out via gradual addition of aliquots of stock solution of the analyte (TATP/picric acid) to the 10 mL of COF dispersed solution and the spectra were recorded 2 min after each addition. The excitation wavelength (λ_{ex}) was at 450 nm and the corresponding emission wavelength was tested from 480 to 800 nm. Each test was repeated at least three times showing reproducible fluorescence intensities. Fluorescence extinction by TATP, with similar efficiency, was also observed for **3BD** and **3′PD** dispersions in diethyl ether; however, no appreciable change of their fluorescence was observed upon addition of TATP to acetonitrile and ethanol dispersion. Also, control experiments with H_2O_2 and *tert*-butyl peroxide (up to 1 mM, in both dichloromethane and diethyl ether) showed no quenching of **3BD** and **3′PD** emission.

ASSOCIATED CONTENT

Supporting Information

The Supporting Information is available free of charge on the ACS Publications website at DOI: 10.1021/jacs.6b12005.

Synthetic procedures and characterization data of the synthesized compounds; Computational protocols, PXRD data, ^{13}C solid-state NMR spectra, BET sorption isotherms, additional SEM and AFM images, chemical stability tests, additional fluorescence sensing and spectroelectrochemical data (PDF)

AUTHOR INFORMATION

Corresponding Author

*dmitrii.perepichka@mcgill.ca

ORCID

Dmitrii F. Perepichka: 0000-0003-2233-416X

Notes

The authors declare no competing financial interest.

ACKNOWLEDGMENTS

This work was supported by NSERC of Canada through Discovery Grant and MESRST of Québec through International Collaboration Grant. MRR thanks FQRNT for PBEEE fellowship. SDF thanks generous support by the Fund of

DOI: 10.1021/jacs.6b12005
J. Am. Chem. Soc. 2017, 139, 2421−2427

Scientific Research − Flanders (FWO), in the framework of a joint project between Flanders and Quebec.

REFERENCES

(1) (a) Côté, A. P.; Benin, A. I.; Ockwig, N. W.; O'Keeffe, M.; Matzger, A. J.; Yaghi, O. M. *Science* **2005**, *310*, 1166. (b) Ding, S.-Y.; Wang, W. *Chem. Soc. Rev.* **2013**, *42*, 548. (c) Waller, P. J.; Gándara, F.; Yaghi, O. M. *Acc. Chem. Res.* **2015**, *48*, 3053. (d) Feng, X.; Ding, X.; Jiang, D. *Chem. Soc. Rev.* **2012**, *41*, 6010. (e) DeBlase, C. R.; Dichtel, W. R. *Macromolecules* **2016**, *49*, 5297.

(2) Doonan, C. J.; Tranchemontagne, D. J.; Glover, T. G.; Hunt, J. R.; Yaghi, O. M. *Nat. Chem.* **2010**, *2*, 235.

(3) (a) DeBlase, C. R.; Silberstein, K. E.; Thanh-Tam, T.; Abruna, H. D.; Dichtel, W. R. *J. Am. Chem. Soc.* **2013**, *135*, 16821. (b) DeBlase, C. R.; Hernández-Burgos, K.; Silberstein, K. E.; Rodríguez-Calero, G. G.; Bisbey, R. P.; Abruña, H. D.; Dichtel, W. R. *ACS Nano* **2015**, *9*, 3178. (c) Xu, F.; Xu, H.; Chen, X.; Wu, D.; Wu, Y.; Liu, H.; Gu, C.; Fu, R.; Jiang, D. *Angew. Chem., Int. Ed.* **2015**, *54*, 6814.

(4) (a) Ding, S.-Y.; Gao, J.; Wang, Q.; Zhang, Y.; Song, W.-G.; Su, C.-Y.; Wang, W. *J. Am. Chem. Soc.* **2011**, *133*, 19816. (b) Fang, Q.; Gu, S.; Zheng, J.; Zhuang, Z.; Qiu, S.; Yan, Y. *Angew. Chem., Int. Ed.* **2014**, *53*, 2878.

(5) (a) Wan, S.; Guo, J.; Kim, J.; Ihee, H.; Jiang, D. *Angew. Chem., Int. Ed.* **2009**, *48*, 8826. (b) Feldblyum, J. I.; McCreery, C. H.; Andrews, S. C.; Kurosawa, T.; Santos, E. J. G.; Duong, V.; Fang, L.; Ayzner, A. L.; Bao, Z. *Chem. Commun.* **2015**, *51*, 13894. (c) Dogru, M.; Handloser, M.; Auras, F.; Kunz, T.; Medina, D.; Hartschuh, A.; Knochel, P.; Bein, T. *Angew. Chem., Int. Ed.* **2013**, *52*, 2920. (d) Calik, M.; Auras, F.; Salonen, L. M.; Bader, K.; Grill, I.; Handloser, M.; Medina, D. D.; Dogru, M.; Löbermann, F.; Trauner, D.; Hartschuh, A.; Bein, T. *J. Am. Chem. Soc.* **2014**, *136*, 17802.

(6) (a) El-Kaderi, H. M.; Hunt, J. R.; Mendoza-Cortés, J. L.; Côté, A. P.; Taylor, R. E.; O'Keeffe, M.; Yaghi, O. M. *Science* **2007**, *316*, 268. (b) Spitler, E. L.; Dichtel, W. R. *Nat. Chem.* **2010**, *2*, 672.

(7) (a) Uribe-Romo, F. J.; Hunt, J. R.; Furukawa, H.; Kloeck, C.; O'Keeffe, M.; Yaghi, O. M. *J. Am. Chem. Soc.* **2009**, *131*, 4570. (b) Chen, X.; Addicoat, M.; Irle, S.; Nagai, A.; Jiang, D. *J. Am. Chem. Soc.* **2013**, *135*, 546. (c) Ascherl, L.; Sick, T.; Margraf, J. T.; Lapidus, S. H.; Calik, M.; Hettstedt, C.; Karaghiosoff, K.; Döblinger, M.; Clark, T.; Chapman, K. W.; Auras, F.; Bein, T. *Nat. Chem.* **2016**, *8*, 310.

(8) Beaudoin, D.; Maris, T.; Wuest, J. D. *Nat. Chem.* **2013**, *5*, 830.

(9) Fang, Q.; Zhuang, Z.; Gu, S.; Kaspar, R. B.; Zheng, J.; Wang, J.; Qiu, S.; Yan, Y. *Nat. Commun.* **2014**, *5*, 4503:1. (b) Fang, Q.; Wang, J.; Gu, S.; Kaspar, R. B.; Zhuang, Z.; Zheng, J.; Guo, H.; Qiu, S.; Yan, Y. *J. Am. Chem. Soc.* **2015**, *137*, 8352.

(10) (a) Vyas, V. S.; Haase, F.; Stegbauer, L.; Savasci, G.; Podjaski, F.; Ochsenfeld, C.; Lotsch, B. V. *Nat. Commun.* **2015**, *6*, 8508:1. (b) Dalapati, S.; Addicoat, M.; Jin, S.; Sakurai, T.; Gao, J.; Xu, H.; Irle, S.; Seki, S.; Jiang, D. *Nat. Commun.* **2015**, *6*, 7786:1. (c) Dalapati, S.; Jin, S.; Gao, J.; Xu, Y.; Nagai, A.; Jiang, D. *J. Am. Chem. Soc.* **2013**, *135*, 17310. (d) Stegbauer, L.; Schwinghammer, K.; Lotsch, B. V. *Chem. Sci.* **2014**, *5*, 2789. (e) Ding, S.-Y.; Dong, M.; Wang, Y.-W.; Chen, Y.-T.; Wang, H.-Z.; Su, C.-Y.; Wang, W. *J. Am. Chem. Soc.* **2016**, *138*, 3031. (f) Kandambeth, S.; Shinde, D. B.; Panda, M. K.; Lukose, B.; Heine, T.; Banerjee, R. *Angew. Chem., Int. Ed.* **2013**, *52*, 13052. (g) Chen, X.; Addicoat, M.; Jin, E.; Zhai, L.; Xu, H.; Huang, N.; Guo, Z.; Liu, L.; Irle, S.; Jiang, D. *J. Am. Chem. Soc.* **2015**, *137*, 3241.

(11) Dou, L.; Liu, Y.; Hong, Z.; Li, G.; Yang, Y. *Chem. Rev.* **2015**, *115*, 12633.

(12) (a) Perepichka, D. F.; Rosei, F. *Science* **2009**, *323*, 216. (b) Gutzler, R.; Perepichka, D. F. *J. Am. Chem. Soc.* **2013**, *135*, 16585.

(13) (a) Grill, L.; Dyer, M.; Lafferentz, L.; Persson, M.; Peters, M. V.; Hecht, S. *Nat. Nanotechnol.* **2007**, *2*, 687. (b) Bieri, M.; Treier, M.; Cai, J.; Aït-Mansour, K.; Ruffieux, P.; Gröning, O.; Gröning, P.; Kastler, M.; Rieger, R.; Feng, X.; Müllen, K.; Fasel, R. *Chem. Commun.* **2009**, *45*, 6919. (c) Gutzler, R.; Walch, H.; Eder, G.; Kloft, S.; Heckl, W. M.; Lackinger, M. *Chem. Commun.* **2009**, *45*, 4456. (d) Cardenas, L.; Gutzler, R.; Lipton-Duffin, J.; Fu, C.; Brusso, J. L.; Dinca, L. E.; Vondráček, M.; Fagot-Revurat, Y.; Malterre, D.; Rosei, F.; Perepichka, D. F. *Chem. Sci.* **2013**, *4*, 3263. (e) Guo, J.; Xu, Y.; Jin, S.; Chen, L.; Kaji, T.; Honsho, Y.; Addicoat, M. A.; Kim, J.; Saeki, A.; Ihee, H.; Seki, S.; Irle, S.; Hiramoto, M.; Gao, J.; Jiang, D. *Nat. Commun.* **2013**, *4*, 2736. (f) Liu, W.; Luo, X.; Bao, Y.; Liu, Y. P.; Ning, G.-H.; Abdelwahab, I.; Li, L.; Nai, C. T.; Hu, Z. G.; Zhao, D.; Liu, B.; Quek, Y. S.; Loh, K. P. *Nat. Chem.* **2017**, DOI: 10.1038/nchem.2696.

(14) Deans, R.; Rose, A.; Bardon, K. M.; Hancock, H. F.; Swager, T. M. *US Patent* 7,799,573 (4/5/07).

(15) (a) Kandambeth, S.; Mallick, A.; Lukose, B.; Mane, V. M.; Heine, T.; Banerjee, R. *J. Am. Chem. Soc.* **2012**, *134*, 19524. (b) Chandra, S.; Kandambeth, S.; Biswal, B. P.; Lukose, B.; Kunjir, S. M.; Chaudhary, M.; Babarao, R.; Heine, T.; Banerjee, R. *J. Am. Chem. Soc.* **2013**, *135*, 17853. (c) Mitra, S.; Kandambeth, S.; Biswal, B. P.; Khayum, M. A.; Choudhury, C. K.; Mehta, M.; Kaur, G.; Banerjee, S.; Prabhune, A.; Verma, S.; Roy, S.; Kharul, U. K.; Banerjee, R. *J. Am. Chem. Soc.* **2016**, *138*, 2823.

(16) No PXRD peaks were observed for **2TPA**.

(17) Nelson, A. P.; Farha, O. K.; Mulfort, K. L.; Hupp, J. T. *J. Am. Chem. Soc.* **2009**, *131*, 458.

(18) (a) Bunck, D. N.; Dichtel, W. R. *J. Am. Chem. Soc.* **2013**, *135*, 14952. (b) Berlanga, I.; Ruiz-González, M. L.; González-Calbet, J. M.; Fierro, J. L. G.; Mas-Ballesté, R.; Zamora, F. *Small* **2011**, *7*, 1207.

(19) Thomas, S. W., III; Joly, G. D.; Swager, T. M. *Chem. Rev.* **2007**, *107*, 1339.

(20) (a) Cotte-Rodriguez, I.; Hernandez-Soto, H.; Chen, H.; Cooks, R. G. *Anal. Chem.* **2008**, *80*, 1512. (b) Askim, J. R.; Li, Z.; LaGasse, M. K.; Rankin, J. M.; Suslick, K. S. *Chem. Sci.* **2016**, *7*, 199. (c) Schulte-Ladbeck, R.; Kolla, P.; Karst, U. *Anal. Chem.* **2003**, *75*, 731. (d) Munoz, R. A. A.; Lu, D.; Cagan, A.; Wang, J. *Analyst* **2007**, *132*, 560.

(21) (a) Lin, G.; Ding, H.; Yuan, D.; Wang, B.; Wang, C. *J. Am. Chem. Soc.* **2016**, *138*, 3302. (b) Das, G.; Biswal, B. P.; Kandambeth, S.; Venkatesh, V.; Kaur, G.; Addicoat, M.; Heine, T.; Verma, S.; Banerjee, R. *Chem. Sci.* **2015**, *6*, 3931.

(22) Patil, A. O.; Heeger, A. J.; Wudl, F. *Chem. Rev.* **1988**, *88*, 183.

(23) (a) Cai, S.-L.; Zhang, Y.-B.; Pun, A. B.; He, B.; Yang, J.; Toma, F. M.; Sharp, L. D.; Yaghi, O. M.; Fan, J.; Zheng, S.-R.; Zhang, W.-G.; Liu, Y. *Chem. Sci.* **2014**, *5*, 4693. (b) Jin, S.; Sakurai, T.; Kowalczyk, T.; Dalapati, S.; Xu, F.; Wei, H.; Chen, X.; Gao, J.; Seki, S.; Irle, S.; Jiang, D. *Chem. - Eur. J.* **2014**, *20*, 14608.

(24) (a) Wang, H.; Helgeson, R.; Ma, B.; Wudl, F. *J. Org. Chem.* **2000**, *65*, 5862. (b) Welch, G. C.; Bazan, G. C. *J. Am. Chem. Soc.* **2011**, *133*, 4632.

DOI: 10.1021/jacs.6b12005
J. Am. Chem. Soc. 2017, 139, 2421−2427